Poly(vinylidene fluoride) (PVDF) Binder Degradation in Li−O₂ Batteries: A Consideration for the Characterization of Lithium Superoxide

Joseph K. Papp,[†,‡] Jason D. Forster,[§] Colin M. Burke,[†,‡] Hyo Won Kim,[†,‡] Alan C. Luntz,[∥,⊥] Robert M. Shelby,[#] Jeffrey J. Urban,[§] and Bryan D. McCloskey*,[†,‡]

[†]Department of Chemical and Biomolecular Engineering, University of California, Berkeley, California 94720, United States

[‡]Energy Storage and Distributed Resources Division, Lawrence Berkeley National Laboratory, Berkeley, California 94720, United States

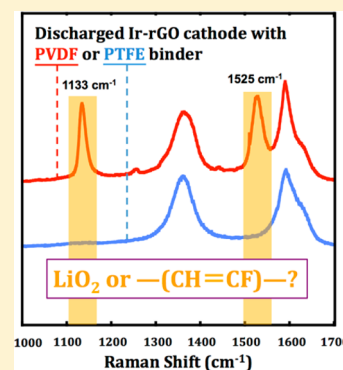[§]The Molecular Foundry, Lawrence Berkeley National Laboratory, Berkeley, California 94720, United States

[∥]SUNCAT Center for Interface Science and Catalysis, Department of Chemical Engineering, Stanford University, Stanford, California 94305, United States

[⊥]SLAC National Accelerator Laboratory, Menlo Park, California 94025, United States

[#]IBM Almaden Research Center, San Jose, California 95120, United States

S *Supporting Information*

ABSTRACT: We show that a common Li−O₂ battery cathode binder, poly(vinylidene fluoride) (PVDF), degrades in the presence of reduced oxygen species during Li−O₂ discharge when adventitious impurities are present. This degradation process forms products that exhibit Raman shifts ($\sim$1133 and 1525 cm^{-1}) nearly identical to those reported to belong to lithium superoxide (LiO₂), complicating the identification of LiO₂ in Li−O₂ batteries. We show that these peaks are not observed when characterizing extracted discharged cathodes that employ poly(tetrafluoroethylene) (PTFE) as a binder, even when used to bind iridium-decorated reduced graphene oxide (Ir-rGO)-based cathodes similar to those that reportedly stabilize bulk LiO₂ formation. We confirm that for all extracted discharged cathodes on which the 1133 and 1525 cm^{-1} Raman shifts are observed, only a 2.0 e$^-$/O₂ process is identified during the discharge, and lithium peroxide (Li₂O₂) is predominantly formed (along with typical parasitic side product formation). Our results strongly suggest that bulk, stable LiO₂ formation via the 1 e$^-$/O₂ process is not an active discharge reaction in Li−O₂ batteries.

Discharged Ir-rGO cathode with PVDF or PTFE binder
1133 cm⁻¹   1525 cm⁻¹
LiO₂ or —(CH=CF)—?
Raman Shift (cm⁻¹)

Lithium-air (Li−O₂) batteries can theoretically provide extraordinarily high specific energy compared with current lithium-ion batteries.[1−3] Unfortunately, their development is inhibited by parasitic reactions that limit cell rechargeability, among other challenges. Although the exact mechanism of the Li−O₂ cathode electrochemistry depends on a variety of cathode and electrolyte properties, the dominant discharge process is oxygen reduction at the cathode to form solid lithium peroxide, Li₂O₂, through a transient superoxide intermediate, for example[4−8]

$$\text{Li}^+ + \text{e}^- + \text{O}_2 \leftrightarrows \text{LiO}_2 \tag{1}$$

$$\text{Li}^+ + \text{e}^- + \text{LiO}_2 \leftrightarrows \text{Li}_2\text{O}_2 \tag{2}$$

or

$$2\text{LiO}_2 \leftrightarrows \text{Li}_2\text{O}_2 + \text{O}_2 \tag{3}$$

The formation and oxidation of Li₂O₂ causes numerous challenges for the development of practical Li−O₂ batteries. Li₂O₂ is a wide bandgap insulator and insoluble in known

organic electrolytes. It therefore greatly limits practical battery capacities by passivating the cathode surface as it is formed.[9−12] It also is highly reactive, resulting in the aforementioned rechargeability limitations.[13−18]

As a result, recent studies have described Li−O₂ cell compositions that may result in the formation of potentially less reactive products and hence may provide a route to improved battery rechargeability.[19,20] Of particular interest, a series of studies have reported a route to stabilizing the lithium superoxide (LiO₂) intermediate such that it comprises a sizable fraction of the ultimate discharge product.[20−23] Using a standard ether-based electrolyte composition, these studies have reported "superoxide-like species" formed on ultrahigh surface area carbon cathodes and pure LiO₂ formation on Ir-decorated reduced graphene oxide (Ir-rGO) electrodes. The most compelling spectroscopic technique employed to identify

the LiO_2 and LiO_2-like species in these studies was ex situ Raman spectroscopy on cathodes extracted from cells after discharge.[20] By combining density functional theory calculations with Raman spectroscopy, two observed peaks (1123 and 1505 cm^{-1}) were ascribed to LiO_2 and LiO_2-like species formation as a discharge product. These ex situ Raman results are unexpected given that bulk LiO_2 has previously been reported to be unstable at room temperature and ambient pressures.[24]

We have briefly noted in review articles that the observation of Raman shifts at similar frequencies (namely, 1125 and 1525 cm^{-1}) was a common, and surprising, occurrence when characterizing cathodes extracted from discharged cells in early Li−O_2 studies.[2,3,25] These studies were performed using a standard cathode composition, namely, carbon black powder (Vulcan XC72) bound to P50 AvCarb carbon paper using a poly(vinylidene fluoride) (PVDF) binder, and a standard ether-based electrolyte. However, we noticed that the Raman peaks at 1125 and 1525 cm^{-1} were not observed if we employed cathode compositions that did not include PVDF. After isolating the cause of these Raman signatures, which we ascribed to PVDF degradation during oxygen reduction in Li−O_2 cells where minor, uncontrolled impurities were present, we changed our binder to poly(tetrafluoroethylene) (PTFE), which eliminated the occurrence of these peaks. Additionally, we determined that the electrode preparation procedure (in particular, the final temperature at which they are dried), which influenced the amount of impurities present after electrode preparation, also influenced the appearance of these peaks when PVDF was used as the binder. In light of recent reports ascribing similar Raman peaks to bulk, stabilized LiO_2 as a final discharge product, this study presents results on PVDF degradation to show how it might be misconstrued as LiO_2 when using Raman spectroscopy studies. Of particular importance, all articles we are aware of in which LiO_2 or LiO_2-like species have been observed as final, stable discharge products use PVDF (Kynar) as a cathode binder.[20−23] In-operando Raman spectroscopy of the Li−O_2 electrochemistry occurring at binder-less glassy carbon and roughened gold electrodes has indeed shown Raman peaks near 1125 and 1525 cm^{-1} that can be ascribed to LiO_2.[7,8,26] However, this LiO_2 is only observed as a *transient, unstable* intermediate to Li_2O_2 formation rather than a stabilized final product.

We study both standard carbon cathodes, such as those prepared from XC72 carbon black bound using PTFE and PVDF, and iridium-decorated reduced graphene oxide (Ir-rGO) electrodes that are similar to those used in a previous study that reports stable bulk LiO_2 formation.[20] Two important results are identified in our study: (1) Raman peaks appear at 1133 and 1525 cm^{-1} only in cells that use PVDF binders and only then if they are not fully dried after preparation under ambient atmosphere. (2) Regardless of the electrode composition employed (binder, catalyst, preparation conditions), we only observe a 2 e^-/O_2 process and never a 1 e^-/O_2 process either on discharge or charge. Our results do not exclude the possibility of a small amount (<1% of total product formation) of LiO_2 formation as possible stable discharge product, and we make no further claim on the possibility of LiO_2 as a stable product. We hope that our results spur further exploration into stable LiO_2 formation, which remains an interesting open question.

Materials. Iridium chloride ($IrCl_3$), ammonium hydroxide (NH_4OH), PTFE emulsion (60 wt %), PVDF ($M_w = 180\,000$

g/mol), N-methyl 2-pyrrolidone (NMP), and sodium hydroxide (NaOH) were all purchased from Sigma-Aldrich. The graphite used as the feedstock for graphene oxide synthesis was acquired from Bay Carbon. 1,2-Dimethoxyethane (DME) and lithium bis(trifluorosulfonylimide) (LiTFSI) were purchased from BASF. P50 Avcarb carbon paper (P50) and XC72 Vulcan carbon black powder (XC72) were purchased from the Fuel Cell Store. Lithium metal was purchased from FMC.

Ir-rGO Synthesis and Characterization. Graphene oxide (GO) was synthesized by a modified Hummer's method, and the Ir-rGO was prepared by a simple thermal reduction method.[27,28] GO was mixed and ultrasonicated in a 300 mL aqueous solution (0.1 wt %), followed by the addition of 100 mg $IrCl_3$ and a repetition of stirring and sonication. 10 mL of 5 M NH_4OH was then added as a reducing agent and the solution was heated to 100 °C for 12 h with a nitrogen atmosphere. After filtering and drying in a vacuum oven at 100 °C, the produced powder was annealed at 450 °C for 3 h under an inert atmosphere (N_2). The final Ir-rGO product was characterized by powder X-ray diffraction (PXRD), transmission electron microscopy (TEM), and X-ray photoelectron spectroscopy (XPS). PXRD (Bruker) was used to determine iridium decoration in rGO and estimate the size of the iridium nanoparticles in the Ir-rGO samples. The PXRD results (Figure 1a) show the appearance of the Ir(111) metal diffraction
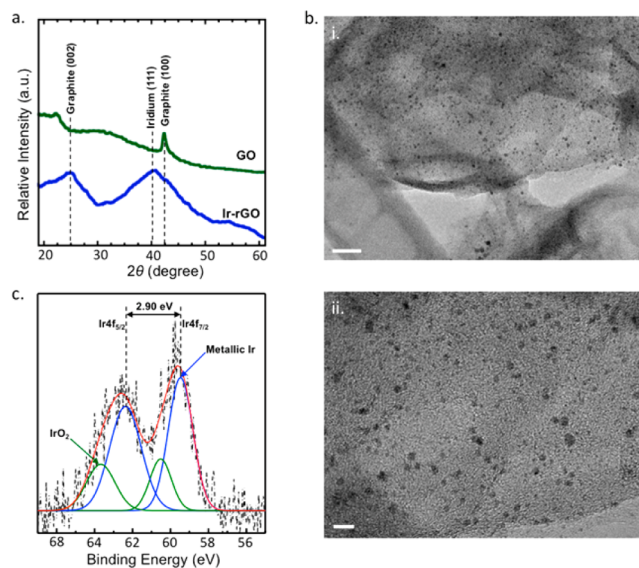
Figure 1. Ir-rGO composition characterization. (a) PXRD results for rGO and Ir-rGO in which the broad peak centered on 40° is evidence of iridium metal formation. (b) TEM images of the prepared Ir-rGO. Iridium nanoparticles are observed as the dark spots in the material. (i) Scale bar 20 nm and (ii) scale bar 5 nm. (c) XPS of the Ir-rGO material. Peak deconvolution confirms the presence of primarily metallic iridium on the reduced graphene oxide, with a small amount of IrO_2 also present.

pattern after the synthesis procedure,[29] without the presence of $IrCl_3$ reflections. An estimation for the size of the iridium nanoparticles based on peak broadening using the Scherrer equation is ~1.5 nm. TEM (JEOL 2100-F 200 kV field-emission analytical transmission electron microscope) was employed to determine the morphology, dispersion, and particle size of the iridium in the Ir-rGO samples. Samples for TEM were prepared by placing a drop of an ultra dilute solution of Ir-rGO on a copper grid that was then dried. TEM

images (Figure 1b) show that the iridium nanoparticles decorating the rGO are well-dispersed and generally very small (<2 nm). X-ray photoelectron spectroscopy (XPS) was carried out to verify the chemical structure of Ir-rGO using a monochromatized Al Kα X-ray source (Quantum2000, Physical electronics, Chanhassen, MN). Figure 1c shows representative XPS spectra of the Ir 4f edge in Ir-rGO, which was then deconvoluted by Gaussian curve fitting. The peaks at 61.2 and 64.1 eV are ascribed to metallic iridium (Ir $4f_{7/2}$ and Ir $4f_{5/2}$), with minor shoulders at 62.6 and 65.7 eV due to the presence of IrO_2.[20] From TEM and XPS data, we confirm that metallic Ir is mainly attached to the basal planes of the rGO. These results confirm that we have synthesized an Ir-decorated reduced graphene oxide material where the Ir metal particles are small (<2 nm) and well-dispersed, as is consistent with a previous study.[20]

Electrode Preparation and Nomenclature. Five different electrodes were studied and are reported using the following naming convention: XXXX/YYYY ZZZZ, where "XXXX" is the active material (either Ir-rGO or Vulcan XC72 carbon black), "YYYY" is the binder used (either PVDF or PTFE), and "ZZZZ" is the final drying temperature used during the electrode preparation process (either 25 or 200 °C).

To prepare electrodes in which PVDF was used as the binder, a homogenized slurry of active materials, binder, and NMP (active material to PVDF weight ratio of 50:50, 10 wt % solids in NMP solution) was evenly spread onto a P50 carbon paper substrate. To prepare electrodes in which PTFE was used as the binder, a homogenized slurry of active materials composed of a PTFE dispersion (60 wt % in H_2O), a 1:1 mixture of isopropanol/H_2O, and Ir-rGO (active material to PTFE weight ratio of 50:50) was spread onto a P50 carbon paper substrate.

Electrodes were then dried using one of two procedures: either by placing them in a fume hood under ambient conditions overnight (electrodes labeled ZZZZ = 25 °C) or by drying under vacuum at 110 °C overnight, quickly transferring them into a glovebox while still hot, and then placing them on a 200 °C hot plate for at least 1 h prior to cell assembly (ZZZZ = 200 °C). No additional drying was performed on the 25 °C electrodes, other than the short exposure to vacuum during antechamber transfer into the glovebox. As will be seen later, the difference in these drying procedure plays a critical role in the Raman spectra of analyzed discharged cathodes. Measured after drying, the electrodes had a typical active material (Ir-rGO or XC72) loading of 2 mg on 12 mm diameter electrodes.

Electrochemical Characterization. Electrochemical cells were assembled in a custom-built modified Swagelok-type cell,[30] with a lithium metal anode (7/16″ diameter), 1 M lithium bis(trifluorosufonyl imide) (LiTFSI) in 1,2-dimethoxyethane as the electrolyte (80 μL), a glass fiber separator (QMA Whatman), and a cathode (12 mm diameter) backed with stainless-steel mesh. Cells were then discharged and charged at a total current of 0.1 mA. Gas consumption and evolution during the electrochemical experiments were monitored using an established pressure decay/rise measurement. Differential electrochemical mass spectrometry (DEMS) was also employed to confirm the analysis provided by pressure monitoring and to quantify individual gases evolved.[30−32] These systems were leak checked by ensuring that the pressure remained stable while the cells were held at open-circuit voltage (OCV) (Figure S1). Well-established iodometric titrations were also used to

quantify Li_2O_2 formation during discharge.[13] Of note, no O_2 evolution was observed from electrodes immersed in water during the titration protocol, indicating that any titrated H_2O_2 was formed from the dissolution of Li_2O_2 and not a reaction involving LiO_2. (O_2 evolution during this titration has been observed when characterizing sodium superoxide, NaO_2, formation in Na−O_2 batteries.[33])

Raman Characterization of Discharged Cathodes. Raman spectra of the discharged cathodes were acquired by use of a Witec alpha300 S confocal Raman microscope with a fiber-coupled laser operating at 532 nm. Samples were prepared for Raman by first disassembling the cells inside an argon filled glovebox and then placing the cathodes in an airtight spectroscopy cell. Prior to placing cathodes in the airtight cells, any residual electrolyte solvent was evaporated from the cathodes using a vacuum antechamber. Typically 10% of the maximum 50 mW laser intensity was applied, with a collection time of 10−30s.

Results and Discussion. A previous report indicated that bulk, stable LiO_2 forms on Ir-rGO-based cathodes.[20] As LiO_2 forms via a $1e^-/O_2$ process (eq 1) and Li_2O_2 forms via a $2e^-/O_2$ process (eqs 1 and 2 and/or eqs 1 and 3), quantitative gas analysis coupled to coulometry was employed to help identify the possible discharge product for cells with Ir-rGO based cathodes. The resulting galvanostatic charge/discharge curves are shown in Figure 2a−c, and the quantification of oxygen consumption and evolution via online pressure monitoring is presented in Figure 2d−i. Regardless of binder employed or cathode preparation conditions, we observe a nearly 2 e^-/O_2 process throughout discharge: 2.00 ± 0.05 for the Ir-rGO/
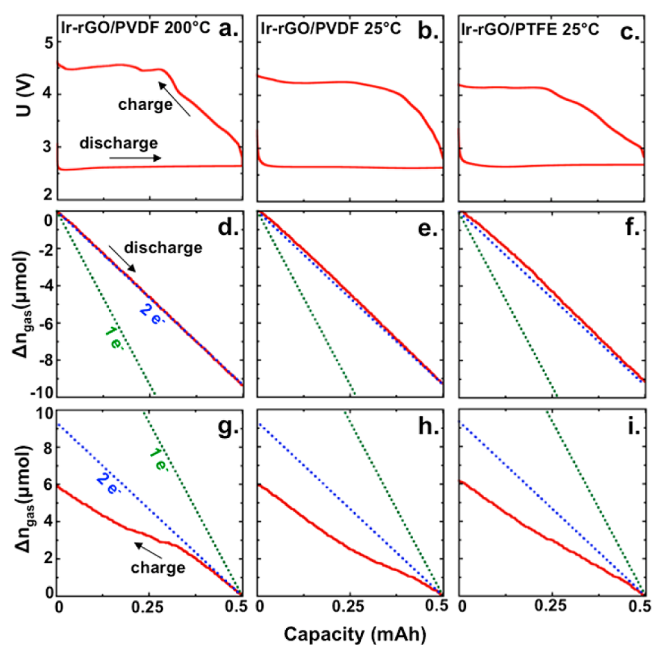
Figure 2. Voltage and gas consumption/evolution plots for Ir-rGO cathodes. (a−c) Galvanostatic discharge/charge curves. (d−f) Gas consumption during discharge under oxygen as measured by pressure decay in an isolated, volume calibrated headspace. (g−i) Gas evolution during charge as measured by pressure rise in the same headspace. Dashed blue and green lines in panels d−i are expected O_2 consumption/evolution profiles for a $1e^-/O_2$ and $2e^-/O_2$ process. Discharge/charge capacity: 0.5 mAh; current density: 100 μA; active material loading: ∼ 2 mg/cm² (12 mm diameter cathode).

PVDF 200 °C cells, 2.01 ± 0.05 for the Ir-rGO/PVDF 25 °C cells, and 2.03 ± 0.05 for the Ir-rGO/PTFE 25 °C cells. The 2 e^-/O_2 ratio is consistent with Li_2O_2 formation as the primary discharge product, although we note that statistical variance in the O_2 consumption measurements does allow for the possibility of perhaps 1 to 2 mol % of the final product to be LiO_2.

Standard analysis of discharged cathodes via PXRD confirmed the expected presence of Li_2O_2 (Figure S2). To further demonstrate the presence of Li_2O_2 as the dominant discharge product, extracted cathodes were immersed in deionized water after a 0.5 mAh discharge, and the resulting H_2O_2 was titrated using established protocol.[13] Li_2O_2 was found to form at a 94% yield in cells similar to those characterized in Figure 2a,d and 90% in cells similar to those in Figure 2b,e. In comparison, cells employing XC72/PVDF and XC72/PTFE cathodes exhibited 88% Li_2O_2 yield, consistent with previous reports.[13] The increase in Li_2O_2 yield when using Ir-rGO as a cathode material indicates that employing Ir-rGO as the cathode material reduces parasitic side reactions involving Li_2O_2 compared with pure carbon cathodes. This observation is somewhat surprising given iridium's ability to dissociate O_2, which could potentially induce additional parasitic reactions. Further study into this Li_2O_2 yield increase on Ir-rGO cathodes is recommended. Of note, no gas evolution was observed during the immersion in water of any of the discharged electrodes. This is an important finding, as we would expect that if LiO_2 was present in the discharged cathodes it would disproportionate to H_2O_2 and O_2 in water in a similar fashion to the disproportionation reaction clearly observed when a similar quantity of NaO_2 is immersed in water.[33]

On charge, while each voltage profile is slightly different, the gas evolution from all cells studied is consistent with previous reports for $Li-O_2$ cells, namely, an initial gas evolution rate close to what is expected (~2 e^-/O_2 process), followed by a deviation away from a 2 e^- process (to higher e^-/O_2 values) throughout charge.[34] This result was confirmed by DEMS analysis, which provided the identification and quantification of gases evolved during charge (Figure S3). In other words, at no point during a typical galvanostatic discharge–charge measurement do we observe a 1 e^-/O_2 or a mixed 1 and 2 e^-/O_2 process in cells employing ether-based electrolytes and Ir-rGO-based cathodes.

Figure 3 presents the Raman spectra of cathodes extracted from cells after large capacity (~10 mAh/cm^2) discharges. The appearance of two peaks at 1133 and 1525 cm^{-1} is highlighted given that similar peaks have been ascribed to LiO_2 formation previously.[20–23] Although these shifts do not precisely align with those reported in previous studies (1123 and 1505 cm^{-1}), we suspect that differences in background subtraction could result in slightly different peak shifts, particularly given the large fluorescent background typically observed during initial illumination. Furthermore, background subtraction could more dramatically influence the peak at 1525 cm^{-1} given that it slightly overlaps with the carbon G-band (1590 cm^{-1}). It is worth noting that peak shifts of 1128 and 1520 ± 2 cm^{-1} were observed in our "uncontrolled impurity" studies (those discussed in the introduction that eventually led to the replacement of PVDF with PTFE as a binder). Importantly, these two peaks only appear in this study when PVDF is used as a binder, regardless of whether Ir-rGO- or XC72-based electrodes are used. When PVDF-bound cathodes are only air-dried during preparation (i.e., Ir-rGO/PVDF 25 °C and XC72/
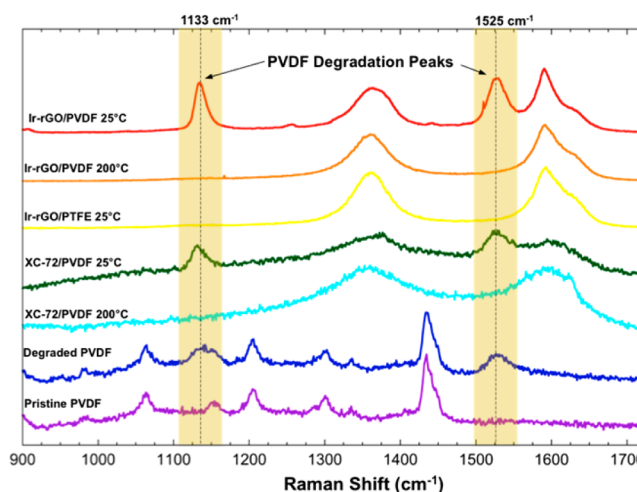
Figure 3. Raman spectra (excitation laser wavelength of 532 nm) of discharged electrodes as well as pristine and alkaline degraded PVDF pellets. For discharged cathodes (top 5 spectra) capacity: ~10 mAh; current density: 100 μA; 12 mm diameter cathodes; ~2 mg active material loading.

PVDF 25 °C), the 1133 and 1525 cm^{-1} peaks are pronounced and ubiquitous after discharge. However, these peaks are not observed if cathodes are rigorously dried prior to cell assembly (Ir-rGO/PVDF 200 °C and XC72/PVDF 200 °C). Changing the binder to PTFE also eliminated the presence of these peaks, regardless of the cathode drying procedure (Ir-rGO/PTFE 25 °C). These results, in combination with the observed 2 e^-/O_2 process on discharge for all cells studied (Figure 2), indicate that the origin of the Raman peaks at 1133 and 1525 cm^{-1} is related to a process involving PVDF degradation and not to the formation of stable LiO_2.

PVDF alkaline "treatment" to improve its surface hydrophilicity is very common, and many previous reports show that such alkaline treatment causes changes in the PVDF surface structure.[35] We confirmed that hydroxyl-induced HF elimination from PVDF is the likely origin of the Raman peaks at 1133 and 1525 cm^{-1}. PVDF pellets were placed in alkaline solution (12 M KOH) for 3 h, rinsed, and then characterized using Raman spectroscopy. Peaks at 1133 and 1525 cm^{-1} are clearly observed ("degraded PVDF" in Figure 3) as a result of a chemical change at the surface of the alkaline-soaked PVDF pellets. (Raman spectra of pure PVDF pellets are also shown in Figure 3.) These peaks have been previously ascribed to the formation of —(CH=CF)— species on PVDF's surface during OH$^-$ attack, with a C–C band at 1127 cm^{-1} and a C=C band at 1525 cm^{-1}.[2,36] Taken together, these observations present compelling evidence that the peaks previously ascribed to LiO_2 are, in fact, due to PVDF binder degradation when small water impurities are present in the cell. Note that in Figure 3 the pristine PVDF peaks are still present for the degraded sample because the depth of Raman sampling is larger than the thickness of the degraded surface layer on the PVDF pellets tested.

In the batteries tested, the cause of the degradation likely stems from the presence of water, NMP, and possible debris on the electrode during preparation that then contributes to the formation of reactive soluble species in the battery. These reactive species then likely attack the PVDF to cause a change in chemical composition that is reflected in the Raman spectra. We have found that this degradation can be avoided by

carefully preparing electrodes to remove and prevent the presence of water and slurry solvents (NMP). Of course, water impurities can accumulate through degradation processes involving the electrolyte or electrode. In fact, we note that the 1133 and 1525 cm^{-1} peaks are occasionally observed in isolated spots at the periphery of the rigorously dried Ir-rGO/PVDF 200 °C cathodes after discharge, presumably resulting from solvent degradation that results in the requisite reactive soluble species necessary to form products that result in these peaks. Because of these occurrences, we encourage any future studies that wish to explore the presence of superoxide-like species to use alternative cathode binders instead of PVDF (e.g., PTFE).

In summary, we have shown that preparation technique and binder selection for Ir-rGO cathodes directly influence the Raman spectra observed upon discharge. We observe a 2.0 e$^-$/O$_2$ processes during discharge for all cells studied, as is consistent with Li$_2$O$_2$ formation. Li$_2$O$_2$ as the dominant discharge product is also supported by titrations performed on discharged electrodes. Charge gas evolution in all cells studied is consistent with previous Li−O$_2$ studies, in which a slightly higher than 2 e$^-$/O$_2$ process is observed initially, followed by a deviation to even higher values as charge proceeds. Despite the electrochemistry pointing toward Li$_2$O$_2$ as the major product, we still find evidence of Raman peaks that were previously ascribed to LiO$_2$, although only in cells that employ PVDF as a cathode binder and where the cathodes are not rigorously dried. Of particular interest, these peaks can be found for both iridium decorated electrodes and ordinary carbon black electrodes. We note slight compositional differences between our cells and those that reportedly resulted in LiO$_2$ formation previously: The preparation procedure of the Ir-rGO is not identical; we employ DME (monoglyme) as an electrolyte solvent rather than tetraethylene glycol dimethyl ether (tetraglyme), and our experimental setups are dissimilar.[30,37] Nevertheless, we believe these slight differences should not result in the dramatic difference in electrochemical behavior reported between our studies. We hope further investigation by others will continue to elucidate the cause of the product differences between this and other studies but emphasize that any spectroscopic characterization absolutely needs to be confirmed with well-established quantitative analysis of gas consumption/evolution and product formation.

■ ASSOCIATED CONTENT

Ⓢ Supporting Information

The Supporting Information is available free of charge on the ACS Publications website at DOI: 10.1021/acs.jpclett.7b00040.

Pressure decay as monitored during OCV and discharge, X-ray diffraction characterization, and DEMS results. (PDF)

■ AUTHOR INFORMATION

Corresponding Author

*E-mail: bmcclosk@berkley.edu.

ORCID Ⓞ

Joseph K. Papp: 0000-0002-7982-6096
Colin M. Burke: 0000-0002-8826-0944
Bryan D. McCloskey: 0000-0001-6599-2336

Notes

The authors declare no competing financial interest.

■ REFERENCES

(1) Christensen, J.; Albertus, P.; Sanchez-Carrera, R. S.; Lohmann, T.; Kozinsky, B.; Liedtke, R.; Ahmed, J.; Kojic, A. A Critical Review of Li/air Batteries. J. Electrochem. Soc. 2012, 159, R1−R30.

(2) Luntz, A. C.; McCloskey, B. D. Nonaqueous Li air Batteries: a Status Report. Chem. Rev. 2014, 114, 11721−11750.

(3) Aurbach, D.; McCloskey, B. D.; Nazar, L. F.; Bruce, P. G. Advances in Understanding Mechanisms Underpinning Lithium−Air Batteries. Nature Energy 2016, 1, 16128.

(4) Aetukuri, N. B.; McCloskey, B. D.; García, J. M.; Krupp, L. E.; Viswanathan, V.; Luntz, A. C. Solvating Additives Drive Solution-Mediated Electrochemistry and Enhance Toroid Growth in Non-Aqueous Li O$_2$ Batteries. Nat. Chem. 2014, 7, 50−56.

(5) Laoire, C. O.; Mukerjee, S.; Abraham, K. M.; Plichta, E. J.; Hendrickson, M. A. Influence of Nonaqueous Solvents on the Electrochemistry of Oxygen in the rechargeable lithium-air battery. J. Phys. Chem. C 2010, 114, 9178−9186.

(6) Laoire, C. O.; Mukerjee, S.; Abraham, K. M.; Plichta, E. J.; Hendrickson, M. A. Elucidating the Mechanism of Oxygen Reduction for Lithium-Air Battery Applications. J. Phys. Chem. C 2009, 113, 20127−20134.

(7) Johnson, L.; Li, C.; Liu, Z.; Chen, Y.; Freunberger, S. A.; Ashok, P. C.; Praveen, B. B.; Dholakia, K.; Tarascon, J.-M.; Bruce, P. G. The Role of LiO$_2$ Solubility in O$_2$ Reduction in Aprotic Solvents and its Consequences for Li−O$_2$ Batteries. Nat. Chem. 2014, 6, 1091−1099.

(8) Peng, Z.; Freunberger, S. A.; Hardwick, L. J.; Chen, Y.; Giordani, V.; Barde, F.; Novak, P.; Graham, D.; Tarascon, J.-M.; Bruce, P. G. Oxygen Reactions in a Non-Aqueous Li$^+$ Electrolyte. Angew. Chem., Int. Ed. 2011, 50, 6351−6355.

(9) Luntz, A. C.; Viswanathan, V.; Voss, J.; Varley, J. B.; Nørskov, J. K.; Scheffler, R.; Speidel, A. Tunneling and Polaron Charge Transport through Li$_2$O$_2$ in Li-O$_2$ Batteries. J. Phys. Chem. Lett. 2013, 4, 3494−3499.

(10) Viswanathan, V.; Thygesen, K. S.; Hummelshoj, J. S.; Norskov, J. K.; Girishkumar, G.; McCloskey, B. D.; Luntz, A. C. Electrical Conductivity in Li$_2$O$_2$ and its Role in Determining Capacity Limitations in Non-Aqueous Li-O$_2$ Batteries. J. Chem. Phys. 2011, 135, 214704.

(11) Hummelshoj, J. S.; Blomqvist, J.; Datta, S.; Vegge, T.; Rossmeisl, J.; Thygesen, K. S.; Luntz, A. C.; Jacobsen, K. W.; Norskov, J. K. Elementary Oxygen Electrode Reactions in the Aprotic Li-Air Battery. J. Chem. Phys. 2010, 132, 071101.

(12) Gerbig, O.; Merkle, R.; Maier, J. Electron and Ion Transport in Li$_2$O$_2$. Adv. Mater. 2013, 25, 3129−3133.

(13) McCloskey, B. D.; Valery, A.; Luntz, A. C.; Gowda, S. R.; Wallraff, G. M.; Garcia, J. M.; Mori, T.; Krupp, L. E. Combining Accurate O$_2$ and Li$_2$O$_2$ Assays to Separate Discharge and Charge Stability Limitations in Nonaqueous Li-O$_2$ Batteries. J. Phys. Chem. Lett. 2013, 4, 2989−2993.

(14) McCloskey, B. D.; Bethune, D. S.; Shelby, R. M.; Mori, T.; Scheffler, R.; Speidel, A.; Sherwood, M.; Luntz, A. C. Limitations in Rechargeability of Li-O$_2$ Batteries and Possible Origins. J. Phys. Chem. Lett. 2012, 3, 3043−3047.

(15) Bryantsev, V. S.; Uddin, J.; Giordani, V.; Walker, W.; Addison, D.; Chase, G. V. The Identification of Stable Solvents for Nonaqueous Rechargeable Li-Air Batteries. *J. Electrochem. Soc.* **2013**, *160*, A160−A171.

(16) Bryantsev, V. S.; Giordani, V.; Walker, W.; Blanco, M.; Zecevic, S.; Sasaki, K.; Uddin, J.; Addison, D.; Chase, G. V. Predicting Solvent Stability in Aprotic Electrolyte Li−Air Batteries: Nucleophilic Substitution by the Superoxide Anion Radical ($O_2\bullet^-$). *J. Phys. Chem. A* **2011**, *115*, 12399−12409.

(17) Leskes, M.; Moore, A. J.; Goward, G. R.; Grey, C. P. Monitoring the Electrochemical Processes in the Lithium−Air Battery by Solid State NMR Spectroscopy. *J. Phys. Chem. C* **2013**, *117*, 26929−26939.

(18) Leskes, M.; Drewett, N. E.; Hardwick, L. J.; Bruce, P. G.; Goward, G. R.; Grey, C. P. Direct Detection of Discharge Products in Lithium−Oxygen Batteries by Solid-State NMR Spectroscopy. *Angew. Chem.* **2012**, *124*, 8688−8691.

(19) Lim, H.-K.; Lim, H.-D.; Park, K.-Y.; Seo, D.-H.; Gwon, H.; Hong, J.; Goddard, W. A., III; Kim, H.; Kang, K. Toward a Lithium-"Air" Battery: The Effect of CO_2 on the Chemistry of a Lithium-Oxygen Cell. *J. Am. Chem. Soc.* **2013**, *135*, 9733−9742.

(20) Lu, J.; Lee, Y. J.; Luo, X.; Lau, K. C.; Asadi, M.; Wang, H. H.; Brombosz, S.; Wen, J.; Zhai, D.; Chen, Z.; et al. A Lithium-Oxygen Battery Based on Lithium Superoxide. *Nature* **2016**, *529*, 377−82.

(21) Zhai, D.; Lau, K. C.; Wang, H. H.; Wen, J.; Miller, D. J.; Lu, J.; Kang, F.; Li, B.; Yang, W.; Gao, J.; et al. Interfacial Effects on Lithium Superoxide Disproportionation in Li-O$_2$ Batteries. *Nano Lett.* **2015**, *15*, 1041−6.

(22) Yang, J.; Zhai, D.; Wang, H. H.; Lau, K. C.; Schlueter, J. A.; Du, P.; Myers, D. J.; Sun, Y. K.; Curtiss, L. A.; Amine, K. Evidence for Lithium Superoxide-like Species in the Discharge Product of a Li-O$_2$ Battery. *Phys. Chem. Chem. Phys.* **2013**, *15*, 3764−71.

(23) Zhai, D.; Wang, H. H.; Lau, K. C.; Gao, J.; Redfern, P. C.; Kang, F.; Li, B.; Indacochea, E.; Das, U.; Sun, H. H.; et al. Raman Evidence for Late Stage Disproportionation in a Li-O$_2$ Battery. *J. Phys. Chem. Lett.* **2014**, *5*, 2705−10.

(24) Andrews, L. Matrix Infrared Spectrum and Bonding in Lithium Superoxide Molecule LiO$_2$. *J. Am. Chem. Soc.* **1968**, *90*, 7368−7370.

(25) McCloskey, B. D.; Burke, C. M.; Nichols, J. E.; Renfrew, S. E. Mechanistic Insights for the Development of Li-O$_2$ Battery Materials: Addressing Li$_2$O$_2$ Conductivity Limitations and Electrolyte and Cathode Instabilities. *Chem. Commun.* **2015**, *51*, 12701−12715.

(26) Galloway, T. A.; Hardwick, L. J. Utilizing in Situ Electrochemical SHINERS for Oxygen Reduction Reaction Studies in Aprotic Electrolytes. *J. Phys. Chem. Lett.* **2016**, *7*, 2119−2124.

(27) Hummers, W. S.; Offeman, R. E. Preparation of Graphitic Oxide. *J. Am. Chem. Soc.* **1958**, *80*, 1339−1339.

(28) Xu, Y.; Sheng, K.; Li, C.; Shi, G. Self-Assembled Graphene Hydrogel via a One-Step Hydrothermal Process. *ACS Nano* **2010**, *4*, 4324−30.

(29) Kumar, S.; Chinnathambi, S.; Munichandraiah, N. Ir Nano-particles-Anchored Reduced Graphene Oxide as a Catalyst for Oxygen Electrode in Li-O$_2$ Cells. *New J. Chem.* **2015**, *39*, 7066−7075.

(30) McCloskey, B. D.; Bethune, D. S.; Shelby, R. M.; Girishkumar, G.; Luntz, A. C. Solvents' Critical Role in Nonaqueous Lithium-Oxygen Battery Electrochemistry. *J. Phys. Chem. Lett.* **2011**, *2*, 1161−1166.

(31) Ma, S. C.; Wu, Y.; Wang, J. W.; Zhang, Y. L.; Zhang, Y. T.; Yan, X. X.; Wei, Y.; Liu, P.; Wang, J. P.; Jiang, K. L.; et al. Reversibility of Noble Metal-Catalyzed Aprotic Li-O$_2$ Batteries. *Nano Lett.* **2015**, *15*, 8084−8090.

(32) Zhang, Y. L.; Cui, Q. H.; Zhang, X. M.; McKee, W. C.; Xu, Y.; Ling, S. G.; Li, H.; Zhong, G. M.; Yang, Y.; Peng, Z. Q. Amorphous Li$_2$O$_2$: Chemical Synthesis and Electrochemical Properties. *Angew. Chem., Int. Ed.* **2016**, *55*, 10717−10721.

(33) McCloskey, B. D.; Garcia, J. M.; Luntz, A. C. Chemical and Electrochemical Differences in Nonaqueous Li O$_2$ and Na O$_2$ Batteries. *J. Phys. Chem. Lett.* **2014**, *5*, 1230−1235.

(34) McCloskey, B. D.; Speidel, A.; Scheffler, R.; Miller, D. C.; Viswanathan, V.; Hummelshøj, J. S.; Nørskov, J. K.; Luntz, A. C. Twin Problems of Interfacial Carbonate Formation in Nonaqueous Li−O$_2$ Batteries. *J. Phys. Chem. Lett.* **2012**, *3*, 997−1001.

(35) Brewis, D. M.; Mathieson, I.; Sutherland, I.; Cayless, R. A.; Dahm, R. H. Pretreatment of Poly(vinyl fluride) and Poly(vinylidene fluoride) with Potassium Hydroxide. *Int. J. Adhes. Adhes.* **1996**, *16*, 87−95.

(36) Ross, G. J.; Watts, J. F.; Hill, M. P.; Morrissey, P. Surface Modification of Poly(vinylidene fluoride) by Alkaline Treatment 1. The Degradation Mechanism. *Polymer* **2000**, *41*, 1685−1696.

(37) Luo, X.; Wu, T.; Lu, J.; Amine, K. Protocol of Electrochemical Test and Characterization of Aprotic Li-O$_2$ Battery. *J. Visualized Exp.* **2016**, e53740.